Model for electron spin resonance in STM noise

Alvaro Caso,[1,2] Baruch Horovitz,[3] and Liliana Arrachea[1]
[1]*Departamento de Física e IFIBA, Universidad de Buenos Aires, Ciudad Universitaria Pabellón I, (1428) Buenos Aires, Argentina*
[2]*Max-Planck-Institut für Physik komplexer Systeme, Nöthnitzer Str. 38, D-01187 Dresden, Germany*
[3]*Department of Physics, Ben Gurion University, Beer Sheva 84105, Israel*
(Received 29 May 2013; revised manuscript received 25 January 2014; published 12 February 2014)

We propose a model to account for the observed ESR-like signal at the Larmor frequency in the current noise scanning tunnel microscope (STM) experiments identifying spin centers on various substrates. The theoretical understanding of this phenomenon, which allows for single spin detection on surfaces at room temperature, is not settled for the experimentally relevant case that the tip and substrate are not spin polarized. Our model is based on a direct tip-substrate tunneling in parallel with a current flowing via the spin states. We find a sharp signal at the Larmor frequency even at high temperatures, in good agreement with experimental data. We also evaluate the noise in presence of an ac field near resonance and predict splitting of the signal into a Mollow triplet.

DOI: 10.1103/PhysRevB.89.075412 PACS number(s): 73.40.Gk, 73.50.Td, 73.63.−b, 74.55.+v

I. INTRODUCTION

Observing and manipulating single spins is of considerable interest in quantum information. A particularly promising method of detecting a single spin on a surface is by using a scanning tunneling microscope (STM) [1]. The technique has been initiated and developed by Y. Manassen and various collaborators and has the appealing feature of being useful at ambient conditions, in contrast to other techniques operating at very low temperatures [2]. It is based on monitoring the noise, i.e., the current-current correlations, in the STM current and observing a signal at the expected Larmor frequency, similar to an electron spin resonance (ESR) experiment, except that here no oscillating field is applied. This phenomenon was demonstrated on an oxidized Si(111) surface [3,4]. Afterwards, it was also observed in Fe atoms [5] on Si(111) as well as on a variety of organic molecules on a graphite surface [6] and on Au(111) surfaces [7–9]. Recent extensions have resolved two resonance peaks on oxidized Si(111) 7×7 surface corresponding to site specific g factors [10,11] and also enabled the observation of the hyperfine coupling [1,12].

The theoretical understanding of the ESR-STM effect is not settled [1]. The emergence of a finite frequency in a steady state stationary situation is a nontrivial phenomenon. An obvious mechanism for coupling the charge current to the spin precession is spin-orbit coupling [13]. It was shown, that an ESR signal is present in the noise of systems with spin-orbit coupling only when the leads are polarized, either for a strong Coulomb interaction [14,15] or for the noninteracting case [15]. This was shown even in linear response [16]. However, it was found that the signal vanishes when the lead polarization vanishes or with parallel polarizations. In the experiments, the leads are very weakly polarized by the magnetic field with polarization parallel to that of the localized spin, hence the ESR signal vanishes within these models [14,15]. It was argued that an effective spin polarization is realized as a fluctuation effect either for a small number of electrons that pass the localized spin in one cycle [17], or due to a long spin correlation time in the leads [1], or to $1/f$ magnetic noise of the tunneling current [18]. These suggestions are based on an exchange interaction between the localized and itinerant electrons, which is phenomenologically modulated by the localized spin precession; however, Refs. [14,15] show that the exchange interaction is not sufficient to produce an ESR signal. It was further shown that spin-orbit coupling in an asymmetric dot can yield an oscillating electric dipole [19]; however, as shown below Eqs. (4) and (6), this is not sufficient to produce an ESR signal. In summary, there is so far no concrete microscopic model that accounts for an ESR-STM effect with nonpolarized leads.

In the present work, we start by showing that the problem of tunneling via spin states in the presence of spin-orbit interaction has strictly no resonance signal; the presence of an electric dipole coupling does not change this conclusion. We then study a model in which an additional direct coupling between the dot and the reservoir is included. Our model is motivated by studies of quantum dots with spin orbit [20] and by STM studies of a two-impurity Kondo system that shows a significant direct coupling between the tip and substrate states [21,22]. We find that the interference of the direct current and the one via the spin does show an ESR signal in the noise, which increases with the direct coupling. This feature is consistent with the unusual nonmonotonic contour plot presented in Refs. [3,4], i.e., the signal is maximized when the STM tip is not directly on the spin center but slightly ($\sim$1 nm) away, so as to maximize an overlap with a surface state of the substrate. The signal intensity relative to the background is small, yet it is sharp even at temperatures much higher than the ESR frequency; the consistency of this behavior with the experimental data is discussed below. Finally, we also evaluate the noise in presence of an ac field near resonance and predict splitting of the signal, analogous to a Mollow triplet in optics [23,24], a splitting that can further test our model.

II. MODEL AND THEORETICAL TREATMENT

The setup we consider consists of a molecule M with spin $1/2$ on a metallic substrate and also in contact with an STM tip as sketched in Fig. 1. The tip and the substrate define two electron reservoirs T, S. The two states of the molecule, associated to the two spin orientations of the molecule have energies separated by a Zeeman splitting due to an external magnetic field $\mathbf{B}_0 = B_0 \mathbf{e}_z$, and are coupled by tunneling

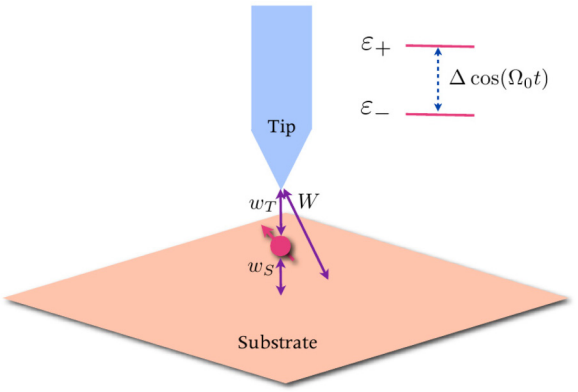

FIG. 1. (Color online) Sketch of the setup. A direct tunneling W takes place between the substrate and the tip. The other transport channel corresponds to two tunneling processes w_S and w_T between the substrate and the molecule and between the tip and the molecule, respectively. In the right-hand side, the effect of a harmonic in time transverse component of the magnetic field that couples the two levels of the molecule is indicated.

processes to the two reservoirs. We assume, in addition, spin-orbit (SO) coupling, which renders these tunneling terms spin dependent, in particular, allowing for tunneling with spin flip. The Hamiltonian is

$$\mathcal{H} = \sum_{\alpha=T,S} \mathcal{H}_\alpha + \mathcal{H}_M + \sum_{\alpha=T,S} \mathcal{H}_{M,\alpha}(t). \tag{1}$$

The first term, with $\mathcal{H}_\alpha = \sum_{k\alpha,\sigma} \varepsilon_{k\alpha} c^\dagger_{k\alpha,\sigma} c_{k\alpha,\sigma}$, corresponds to the unpolarized reservoirs where $\sigma = \pm$ is a spin index. The molecule is described by the simple model

$$\mathcal{H}_M(t) = \sum_{\sigma=\pm} \varepsilon_\sigma d^\dagger_\sigma d_\sigma + \mathbf{B}(t)\cdot\mathbf{s}, \tag{2}$$

with the energy of two spin orientations separated by the Zeeman splitting $\varepsilon_\pm = \pm\omega_z/2$. We also consider a time-dependent component $\mathbf{B}(t)$ in the external magnetic field, while

$$s_j = \frac{1}{2}\sum_{\sigma,\sigma'} d^\dagger_\sigma \hat{\sigma}^j_{\sigma,\sigma'} d_\sigma, \tag{3}$$

being $\hat{\sigma}^j$, $j = x,y,z$ the Pauli matrices. The last term of $\mathcal{H}$ is the coupling to the reservoirs,

$$\mathcal{H}_{M,\alpha} = w \sum_{k\alpha,\sigma,\sigma'} \left(c^\dagger_{k\alpha,\sigma} U^{\alpha\dagger}_{\sigma,\sigma'} d_{\sigma'} + \text{H.c.}\right), \tag{4}$$

where U^α are SU(2) matrices for $\alpha = T,S$, which represents a general spin-orbit coupling [13,15]. In Appendix A, we demonstrate a derivation of such a tunneling matrix. The unitarity of the marices U^α follows in fact from time reversal symmetry $\hat{T}$. Our eigenstates $|\pm\rangle$ are those of the first term of Eq. (2), which is odd under $\hat{T}$, hence $|\pm\rangle$ are nondegenerate with eigenvalues $\pm\frac{1}{2}B_0$ and therefore related by $\hat{T}|\pm\rangle = \pm|\mp\rangle$. Since U^α represents a $\hat{T}$ invariant operator $U^\alpha_{++} = U^{\alpha *}_{--}$, $U^\alpha_{+-} = -U^{\alpha *}_{-+}$, i.e., U^α are SU(2) matrices, up to a prefactor w, in general, α dependent.

Let us now notice that the above Hamiltonian does not contain the minimum ingredients to describe the ESR-STM effect. In fact, the unitary transformation $c'_{k\alpha,\sigma} = \sum_{\sigma'} U^\alpha_{\sigma,\sigma'} c_{k\alpha,\sigma'}$ diagonalizes in spin the tunneling Hamiltonian while leaves unchanged the Hamiltonians of the unpolarized reservoirs. The result is

$$\mathcal{H}_{M,\alpha} = w \sum_{k\alpha,\sigma} (c'^\dagger_{k\alpha,\sigma} d_\sigma + \text{H.c.}). \tag{5}$$

Hence the full Hamiltonian is a sum over two decoupled spin states and observables such as current noise cannot present any feature depending on the level spacing in the molecule, as previously noted in a detailed calculation [15].

The next ingredient to explore is a molecular electric dipole $e\mathbf{r}$ that couples to an electric field $\mathbf{E}$, e.g., due to tip proximity [19]. Assuming a molecule with several levels, in the absence of $\mathbf{E}$, $\mathcal{H}_M$ has eigenstates $|m,\sigma\rangle$ with eigenvalues $E_m \pm \frac{1}{2}\omega_{z,m}$ ($m = 0$ is the ground state), where $\omega_{z,m}$ is the splitting due to a Zeeman term $\mathcal{H}_Z$. Extending the one-dimensional model [19], the oscillating electric dipole $\sim e^{-i\omega_{z,0}t}$ can be described by the second-order matrix element

$$\sum_{m\neq 0} \frac{\langle 0,-|\mathbf{E}\cdot\mathbf{r}|m,-\rangle\langle m,-|\mathcal{H}_Z|0,+\rangle}{E_0 - E_m}, \tag{6}$$

where the asymmetry of the molecule allows for $\langle m,-|\mathcal{H}_Z|0,+\rangle \neq 0$ for $m \neq 0$. Adding this off-diagonal term to $\mathcal{H}_M$ results in eigenstates related to $|0,\pm\rangle$, i.e., d_σ, by a unitary spin rotation. Thus the two spin channels become effectively decoupled and we conclude that the dipole coupling is not sufficient to explain the ESR-STM effect. Choosing a coherent superposition of $|0,\pm\rangle$ states can lead to an oscillating electric dipole $\sim e^{-i\omega_{z,0}t}$ as in (6), yet the average on reservoir states is not sensitive to this coherence and an additional modulation of the tunnel barrier is needed [19] to observe the ESR-STM phenomenon.

Then, we keep considering the simple Hamiltonian (2) for the molecule and we proceed to introduce the main feature of our model. Namely, a direct tunneling between the tip and substrate so that the Hamiltonian (1) acquires an additional term

$$\mathcal{H}_{TS} = W \sum_{kT,k'S,\sigma,\sigma'} \left(c^\dagger_{kT,\sigma} U^{TS}_{\sigma,\sigma'} c_{k'S,\sigma'} + \text{H.c.}\right), \tag{7}$$

where U^{TS} is an SU(2) matrix. This direct tunneling is a generic process that may be present in many STM experiments on molecules on metallic substrates. Its main effect is to generate a transport channel which interferes with the one through the molecule. This interference was found to play an important role in Kondo-correlated molecules and quantum dots [20–22] but so far it has not been explored in the scenario relevant for the ESR phenomena observed in STM noise. Below, we show that for $W \gg w$, this mechanism accounts for the features observed in such experiments.

In terms of the operators $c'_{k\alpha,\sigma}$ previously defined, $\mathcal{H}_{TS}$ involves the SU(2) matrix $\tilde{U}^{TS} = U^T U^{TS} U^{S\dagger}$, which can be written as a general rotation of the form [25] $\tilde{U}^{TS} = U^{\text{SO}} U^\theta$ with

$$U^{\text{SO}} = e^{i\sigma_z\phi_1}, \quad \text{and} \quad U^\theta = e^{i\sigma_z\phi_2/2} e^{i\sigma_y\theta/2} e^{-i\sigma_z\phi_2/2}, \tag{8}$$

where $\sigma_{x,y,z}$ are the Pauli matrices. In terms of the unitary transformation $c''_{kS,\sigma} = \sum_{\sigma'} U^\theta_{\sigma,\sigma'} c'_{kS,\sigma'}$, the direct TS coupling

becomes spin diagonal with the matrix U^{SO} while $\mathcal{H}_{M,S}$ becomes off diagonal with U^{θ}. The phase ϕ_2 can be eliminated by defining $d_\sigma = e^{i\sigma\phi_2/2}\tilde{d}_\sigma$, $c'_{kT,\sigma} = e^{i\sigma\phi_2/2}\tilde{c}_{kT,\sigma}$ and $c''_{kS,\sigma} = e^{i\sigma\phi_2/2}\tilde{c}_{kS,\sigma}$. The different Hamiltonian terms become

$$\begin{aligned}\mathcal{H}_{TS} &= W\sum_{kT,k'S,\sigma}(\tilde{c}^{\dagger}_{kT,\sigma}e^{i\sigma\phi_1}\tilde{c}_{k'S,\sigma} + \text{H.c.}),\\ \mathcal{H}_{M,T} &= w\sum_{kT,\sigma}(\tilde{c}^{\dagger}_{kT,\sigma}\tilde{d}_\sigma + \text{H.c.}),\\ \mathcal{H}_{M,S} &= w\sum_{kS,\sigma,\sigma'}[\tilde{c}^{\dagger}_{kS,\sigma}(e^{i\sigma_y\theta/2})_{\sigma,\sigma'}\tilde{d}_{\sigma'} + \text{H.c.}],\end{aligned} \tag{9}$$

while the $\mathcal{H}_T$,$\mathcal{H}_S$ terms of (1) remain unchanged with the $\tilde{c}_{k\alpha,\sigma}$,$\tilde{d}_\sigma$ operators. The phase θ represents the off-diagonal spin-orbit coupling. For $\theta = 0$ the (rotated) spin states decouple and the ESR effect vanishes as in the $W = 0$ case above. Hence both the spin-orbit coupling with $\theta \neq 0$ and $W \neq 0$ are essential for producing the interference between the tunneling via the spin states and the direct tunneling. We present bellow compelling evidence that this interference can be the mechanism responsible for the ESR-STM effect.

A. Current and noise

For this model, the charge current operator flowing into the tip reads $\hat{J}_T(t) = \hat{J}_{M\to T}(t) + \hat{J}_{S\to T}(t)$, where the first term corresponds to the current flowing through the molecule, while the second one is due to the direct tunneling W,

$$\begin{aligned}\hat{J}_{M\to T}(t) &= i\,w\sum_{kT,\sigma,\sigma'}(\tilde{c}^{\dagger}_{k\alpha,\sigma}(t)\tilde{d}_\sigma(t) - \text{H.c.}),\\ \hat{J}_{S\to T}(t) &= i\,W\sum_{kT,kS,\sigma}(\tilde{c}^{\dagger}_{kT,\sigma}(t)e^{i\sigma\phi_1}\tilde{c}_{kS,\sigma}(t) - \text{H.c.}).\end{aligned} \tag{10}$$

Since the molecule can change its charge, the currents $J_{M\to T}$ and $J_{M\to S}$ may differ. The relevant circuit current depends then on both currents, depending on the ratio of the relevant capacitances [26]. We expect the T-M capacitance to be smaller than the M-S one [27], hence the circuit current [26] is dominated by the tip current $\hat{J}_T$.

The corresponding noise spectrum can be decomposed as $\mathcal{S}(t,\omega) = \mathcal{S}_M(t,\omega) + \mathcal{S}_W(t,\omega)$. The first term corresponds to current-current correlation functions involving current operators through the molecule, while the second one corresponds to those due to the direct current between tip and substrate,

$$\begin{aligned}\mathcal{S}_M(t,\omega) &= \int_{-\infty}^{+\infty}d\tau\langle\hat{J}_T(t)\hat{J}_{M\to T}(t-\tau)\\ &\quad + \hat{J}_{M\to T}(t)\hat{J}_T(t-\tau)\rangle e^{i\omega\tau},\\ \mathcal{S}_W(t,\omega) &= 2\int_{-\infty}^{+\infty}d\tau\langle\hat{J}_{S\to T}(t)\hat{J}_{S\to T}(t-\tau)\rangle e^{i\omega\tau}.\end{aligned} \tag{11}$$

In what follows, we focus on the first term, which contains the relevant information involving the scattering processes through the molecule. The second one represents a background signal, which is usually subtracted from the experimental data. The current is induced by applying a dc bias voltage V, which relates the chemical potentials of the tip and substrate as $\mu_{T,S} = \mu \mp eV/2$. In this stationary case $\mathcal{S}_l(t,\omega) \equiv \mathcal{S}_l(\omega)$, $l = W,M$.

We use the Schwinger-Keldysh Green's functions formalism as the framework to analyze the out-of-equilibrium dynamics of this system. For some details on the calculation and the explicit expressions of the noise spectrum for this particular problem see Appendix B.

III. RESULTS

A. Static magnetic field

We start by analyzing the setup with a static external magnetic field $\mathbf{B}_0$ but without any time-dependent component $\mathbf{B}(t) = 0$. Consider now the experimentally relevant parameters. The dc current $I = \langle\hat{J}_T\rangle \sim 0.1$–1 nA for $V \approx 1$ V [1]. In our model, we find that the Larmor frequency appears in the noise when $W \gg w$, hence the dc conductance is dominated by the W term. The latter is [28] $G_W = \frac{2e^2}{h}\frac{4x}{(1+x)^2}$, where $x = \pi^2 W^2 N_T N_S$ and $N_{T,S}$ are the tip and substrate density of states, taken as constants in the (μ_T,μ_S) range. Assuming $N_{T,S} \sim 1/b$, where b is the bandwidth of these reservoirs, we estimate $W/b \approx 10^{-3}$ corresponding to a weak tunneling regime with $x \ll 1$. The resonance is sharp, with a width of $\Delta\omega/2\pi \approx 1$ MHz [1], much smaller than the resonance frequency, typically $\omega_z/2\pi \approx 500$ MHz. A golden rule estimate, consistent with our data for small w,W, gives a resonance width $\Delta\omega = 2\pi w^2/b$, hence $w/b \approx 10^{-5}$, assuming $b \approx 5$ eV. We find that the width (and amplitude) of the resonance scales in fact as $w_S w_T$, allowing for different tunneling couplings to the tip and substrate w_T and w_S, respectively. If the molecule is close to the substrate $w_S \gtrsim W$ is plausible so that $w_T/W \lesssim 10^{-4}$, consistent with the tip being located about 1 nm sideways from the spin center [3,4].

We note that the experiments were at room temperature, $T \gg \omega_z$, hence the linewidth is not sensitive to temperature. We assume that the chemical potential of the substrate $\mu_S = 0$ lies between the two levels. Our results depend weakly on the position of these levels, as long as at least one of them is in between μ_S and μ_T.

We now show results for the noise spectrum in our model. We have calculated $\mathcal{S}_M(\omega)$ and $\mathcal{S}_T(\omega)$ following the procedure of Ref. [29]. We use $\theta = \pi$ and $\phi_1 = \pi/2$ to maximize the resonance effect (the value of ϕ_1 is irrelevant to the resonance effect). We chose $W,w,T,eV,\epsilon_\pm$ not too far from the experimental estimates (in eV). Both reservoirs are modeled as semi-infinite 1D chains with bandwidth b so that $x = (4W/b)^2$.

Figure 2(a) shows the onset of the Larmor frequency in the noise $\mathcal{S}_M$ as the direct coupling W is turned on. We see that for the experimental estimated value for $W/w = 100$, a sharp peak is clearly distinguished in the noise spectra. This signal persists for all finite W/w as seen in Fig. 2(b), showing the amplitude of the signal as a function of x, the background noise and the classical shot noise $2eI$. The background noise is taken as the mean in the range $\omega_z \pm 0.1\omega_z$, where the noise varies by less than 0.05%. We note that for $x \ll 1$ or $x \gg 1$ the background is the classical shot noise $\mathcal{S}_W + \mathcal{S}_M \approx 2eI$. The current ratio is $\langle J_{M\to T}\rangle/\langle J_{S\to T}\rangle \approx 4\pi w^2/(bxeV)$ (for $x \ll 1$), which for the parameters of Fig. 2(b) is $\approx 10^{-4}/x$. Hence, at $x < 10^{-4}$, the current, as well as the background noise, is dominated by

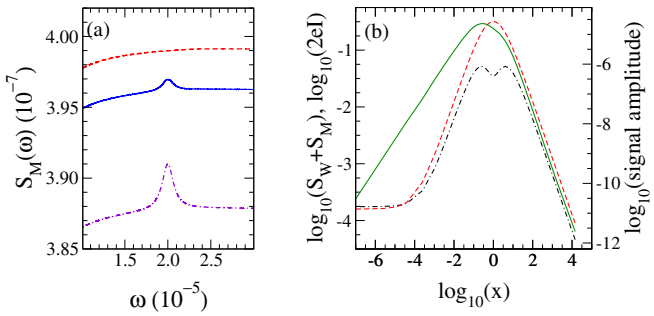

FIG. 2. (Color online) (a) Noise spectrum $\mathcal{S}_M$ for various direct couplings W between reservoirs: 0 (dashed red), 0.05 (solid blue), and 0.1 (dash-dotted violet). The parameters are $\mu = 0.25, eV = 0.5$, $T = 0.05$, $w = 5 \times 10^{-4}$, $\epsilon_\pm = \pm 10^{-5}$, and $b = 5$. (b) Amplitude of the signal at the Larmor frequency (solid green), the background noise $\mathcal{S}_W + \mathcal{S}_M$ (dot-dashed black), and $2eI$ (dashed red) as functions of x. The parameters are $w = 0.01$, $\epsilon_\pm = \pm 5 \times 10^{-3}$, and the other parameters as in (a).

that via the molecule and becomes x independent. The case $x = 1$ corresponds to perfect ballistic matching between the reservoirs, accounting for the maxima in the figure.

Figure 2(b) shows that the signal intensity at $x \ll 1$ is linear with x, same as $\mathcal{S}_W \sim G_W \sim x$. The signal to background ratio at $x = 0.01$ is $\sim 10^{-3}$. Scaling to $w = 5 \times 10^{-5}$ reduces this ratio to $\sim 10^{-8}$. For this w, the background S_W dominates, hence the ratio above is x independent and applies to the experimental situation.

The temperature dependence is shown in Fig. 3. The resonance itself is not sensitive to temperature [see Fig. 3(b)], consistent with the experimental data [1]. In the case of $T = 0$ there are features of the noise spectrum (steps) at the frequencies corresponding to the molecular levels $\varepsilon_\pm$, which are typical of the noise spectrum of two-level systems [30]. These features are washed up by thermal fluctuations as soon as $T > \omega_z$. The dip at $\omega = 0$ is similar to the one seen in Ref. [30], with the latter due to charge conservation at the molecule. Further details on the behavior of the dc noise in the present model can be found in a complementary paper [31].

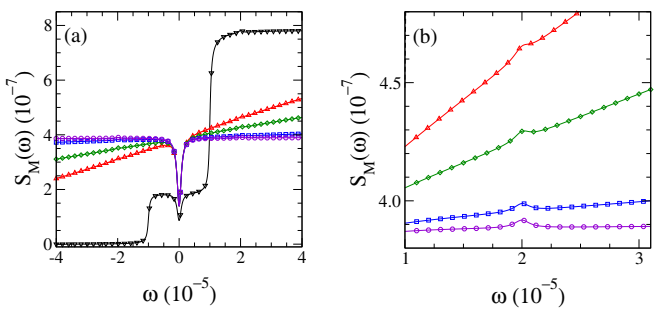

FIG. 3. (Color online) Noise spectrum $\mathcal{S}_M$ at various temperatures T: 0 (black triangles down), 5×10^{-5} (red triangles up), 10^{-4} (green diamond), 5×10^{-4} (blue squares), and 5×10^{-3} (violet circles). Parameters are $W = 0.1$ and those in Fig. 2(a). (b) A magnified part of (a) in the resonance vicinity.

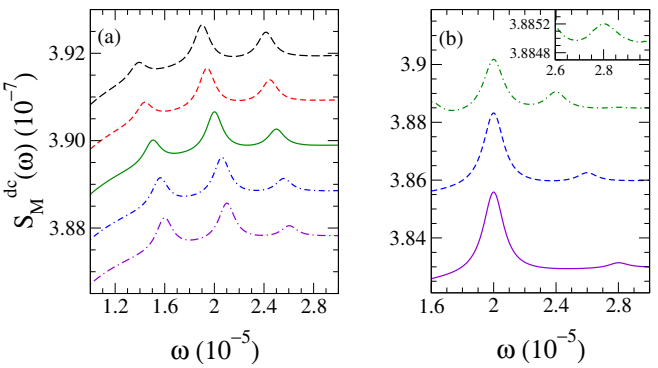

FIG. 4. (Color online) (a) Noise spectrum $\mathcal{S}_M^{\rm dc}$ for perpendicular ac field amplitude $\Delta_\perp = 5 \times 10^{-6}$ and various frequencies Ω_0: 1.9×10^{-5} (long-dashed black), 1.94×10^{-5} (dashed red), 2×10^{-5} [resonant] (solid green), 2.06×10^{-5} (dashed-dotted blue), and 2.1×10^{-5} (long-dashed-dotted violet). (b) Noise spectrum $\mathcal{S}_M^{\rm dc}$ for parallel ac field amplitude $\Delta_\parallel = 2 \times 10^{-6}$ and various frequencies Ω_0: 4×10^{-6} (dashed-dotted green), 6×10^{-6} (dashed blue), and 8×10^{-6} (solid violet). (Inset) Second harmonic corresponding to $\Omega_0 = 4 \times 10^{-6}$. The parameters are $W = 0.1$ and those in Fig. 2(a). The curves below the top one in (a) and (b) are displaced in height for clarity.

B. Time-dependent magnetic field

We now consider the case where the external magnetic field has a static $\mathbf{B}_0$ component as well as an ac one $\mathbf{B}(t)$. In Fig. 4(a), we show the noise in presence of an additional ac magnetic field perpendicularly to the static component, $\mathbf{B}(t) = \Delta_\perp \cos(\Omega_0 t)\mathbf{e}_x$ that induces transitions between the molecule levels. For the isolated molecule, the transition amplitude at time t is

$$\langle -,t|+,t=0\rangle = \frac{\Delta_\perp}{a} e^{-\frac{1}{2}i\Omega_0 t} \sin\left(\frac{1}{2}at\right), \qquad (12)$$

where $a = \sqrt{(\Omega_0 - \omega_z)^2 + \Delta_\perp^2}$ is the Rabi frequency. In the presence of $\Delta_\perp(t)$, the current-current correlation functions (11) depend on the time argument t. In what follows, we consider the ensuing dc components

$$\mathcal{S}_l^{\rm dc}(\omega) = \frac{\Omega_0}{2\pi} \int_0^{\Omega_0/(2\pi)} dt \mathcal{S}_l(t,\omega). \qquad (13)$$

In the present case, we resort to the nonequilibrium Green function formalism of Ref. [32] to evaluate this function (see also Appendix B for some particular details on this calculation). Figure 4(a) shows splitting of the line into three signals located at Ω_0 and $\Omega_0 \pm a$. Our current correlation corresponds to a spin-spin correlation that is not common in ESR measurements. There is, however, an optical analog of light scattering from a two-level atom showing a "Mollow triplet" [23,24]. The observation of this triplet in our spin system is a sensitive test of our model. We show that the observation of these features is robust against changes of the mean chemical potential μ and that against changes in the frequency Ω_0 of the oscillating magnetic field, even away from the resonant condition.

Figure 5(a) shows the dependence on the mean chemical potential μ of the signal amplitudes of the three Mollow

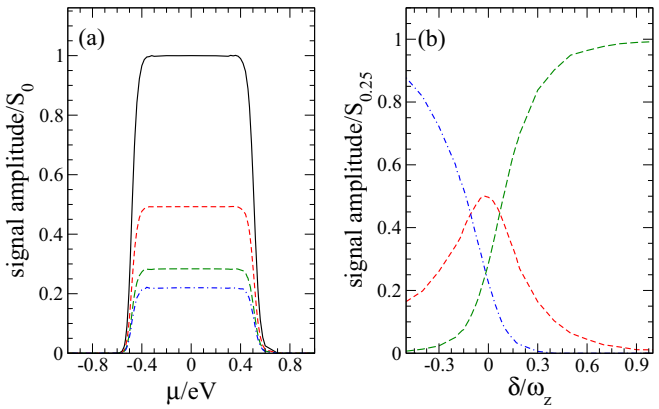

FIG. 5. (Color online) (a) Amplitude of the signal in the absence of an ac field (solid black) along with the amplitudes of the three Mollow peaks located at $\Omega_0 - a$ (long-dashed green), Ω_0 (dashed red), and $\Omega_0 + a$ (dashed-dotted blue) as functions of the mean chemical potential μ. The plot is for the resonant frequency $\Omega_0 = \omega_z$. The amplitudes are normalized to the amplitude of the dc signal for $\mu = 0$ (S_0). Parameters are $T = 0.0125$, $w = 3 \times 10^{-4}$, $W = 0.1$ and those in Fig. 2(a). (b) Amplitudes of the three Mollow peaks located at $\Omega - a$ (long-dashed green), Ω_0 (dashed red), and $\Omega_0 + a$ (dashed-dotted blue) as functions of the detuning δ. The amplitudes are normalized to the amplitude of the dc signal for $\mu = 0.25$ ($S_{0.25}$). Parameters are $\mu = 0.25$ and those in (a).

peaks for a resonant frequency $\Omega_0 = \omega_z$; note that the two localized levels have average 0. We also show for comparison the corresponding signal for the case of a magnetic field without ac component. The signals with and without the ac field have similar dependence on μ showing that the signals are insensitive to the location of the localized levels as long as these are in between the chemical potentials of the tip and substrate. The intensity decays on a scale $\sim T$ when the levels cross either chemical potential. A similar behavior for the case of a magnetic field with dc component only was found in Ref. [31]. We note a "sum rule", i.e., the amplitudes of the three signals in the presence of the ac field add up to the amplitude of the dc signal. It is interesting to notice that the satellite peaks at $\Omega_0 \pm a$ have a slightly different amplitude; this asymmetry is caused by the proximity of the signals to the sharp dip in the noise spectrum at $\omega = 0$ [see Fig. 3(a)], which causes a slowly changing background at the signal positions [see Fig. 4(a)]. As the ratio between the resonance frequency and the width of the signal is increased the background becomes more flat and the asymmetry is reduced. In Fig. 5(a), this ratio is $\approx$30 while under experimental conditions [1] it is $\approx$500, hence we expect symmetric satellites at resonance with the experimental parameters.

In Fig. 5(b), we analyze the effect of a detuning of the frequency of the ac field away from resonance, $\delta = \Omega_0 - \omega_z$. We show the amplitude of the signals of the three Mollow peaks as a function of this parameter. We note that the bare Rabi frequency $\Delta_\perp$ sets the scale of the detuning where the triplet feature is prominent. When $|\delta| > \Delta_\perp$, two peaks are diminishing rapidly and only the peak approaching ω_z survives. Hence the ac field is ineffective at $|\delta| \gg \Delta_\perp$ and the noise reduces to that of the dc case. There is a small asymmetry around $\delta = 0$ as discussed above, e.g., the middle peak is maximized slightly below $\delta = 0$. Also here the asymmetry is reduced when the ratio between the resonance frequency and the width of the signal increase, hence this plot is expected to be symmetric around $\delta = 0$ under experimental conditions. The signal dependence on detuning has been significant for analyzing the type of relaxation mechanism in the optical experiments [23,24].

In Fig. 4(b), we show the noise in presence of an ac magnetic field parallel to the static component, $\mathbf{B}(t) = \Delta_\parallel \cos(\Omega_0 t)\mathbf{e}_z$, which produces an oscillation in the energy levels around their equilibrium values with amplitude $\Delta_\parallel$ and frequency Ω_0. In this case, the time evolution of the off diagonal σ_1 element is

$$e^{i\int_0^t(\omega_z+\Delta_\parallel\cos(\Omega_0 t'))dt'} = e^{i\omega_z t}\sum_{n=-\infty}^{\infty} J_n\left(\frac{\Delta_\parallel}{\Omega_0}\right)e^{in\Omega_0 t}, \quad (14)$$

where $J_n(x)$ are the Bessel functions. For $\Delta_\parallel \ll \Omega_0$ only the first terms of the series with $n = 0, \pm 1$ contribute, as illustrated in Fig. 4(b), where the main peak and the right satellite are shown for several values of Ω_0; the inset zooms on the weaker second-order satellite at $\omega_z + 2\Omega_0$. A case with many sidebands was in fact studied by ESR-STM [5] and is consistent with Eq. (14). It is remarkable that these well-known features from ESR are reproduced in the current noise spectra.

IV. SUMMARY AND CONCLUSIONS

Our model assumes that the spin-orbit interaction is significant, for at least one of the tunneling terms. We note that the strong electric field near the tip can enhance any of the spin-orbit couplings. We consider now several unusual features of the data that our model can account for: (i) a sharp resonance even at high temperatures $T \gg \omega_z$, (ii) insensitivity to the details of the spin defect, i.e., to the positions of its levels between the tip and substrate chemical potentials, (iii) contour plots [3,4] showing that the signal is maximal at $\sim$1 nm from a center, hence a significant direct coupling W bypassing the spin can be achieved. (iv) We account for the ESR-STM phenomenon with unpolarized tip or substrate, in contrast with previous models [14,15] that require polarized leads.

We note that the background noise is not measured in the experiment since the modulation technique [1] measures the derivative of the noise spectra. Furthermore, the signal intensity is under study [12] as it is highly sensitive to uncertainties in the feedback and impedance matching circuits. We estimate that the signal to background intensity is $\sim 10^{-8}$ as discussed above. Furthermore, we predict the appearance of triplet lines when adding a time dependent field perpendicular to the DC one. This phenomena, analogous to the Mollow triplet in optics, provides a sensitive test of our model. We also predict multiple sidebands for modulation with parallel field, partly seen in experiment [5]. In conclusion, our model presents a solution to a long standing puzzle, paving the way for more controlled single spin detection via ESR-STM.

ACKNOWLEDGMENTS

We thank for stimulating discussions with Y. Manassen, C. Berthod, A. Golub, S. A. Gurvitz, A. Janossy, L. S. Levitov, I. Martin, M. Y. Simmons, F. Simon, E. I. Rashba,

S. Rogge, E. A. Rothstein, A. Shnirman, G. Zárand, and A. Yazdani. This research was supported by THE ISRAEL SCIENCE FOUNDATION (BIKURA) (Grant No. 1302/11), by the Israel-Taiwanese Scientific Research Cooperation of the Israeli Ministry of Science and Technology (BH), as well as CONICET, MINCyT, and UBACyT from Argentina (LA and AC).

APPENDIX A: BARDEEN'S FORMULA

Following Bardeen's derivation for tunneling [33], we extend it to allow for spin-orbit coupling, e.g., of the Rashba type. Consider the following Hamiltonians for the tip and the substrate:

$$\begin{aligned}\mathcal{H}_T &= \frac{\hat{p}^2}{2m} + U_T(x)\theta(-x),\\ \mathcal{H}_S &= \frac{\hat{p}^2}{2m} + [U_S(x) + \alpha\,\hat{p}\cdot E\times\sigma]\theta(x), \qquad \text{(A1)}\\ \mathcal{H}_T\varphi_\lambda(x) &= \epsilon_\lambda\varphi_\lambda(x),\ \mathcal{H}_S\varphi_\rho(x) = \epsilon_\rho\varphi_\rho(x).\end{aligned}$$

$x = 0$ defines a surface, not necessarily planar, α is the spin-orbit coupling, E is an electric field (could be external), σ is the spin operator, e.g., Pauli matrices for spin $\frac{1}{2}$, and $\varphi_\lambda(x)$,$\varphi_\rho(x)$ are spinors.

A perturbation correction to $\varphi_\lambda(x)$ yields the tunneling element

$$w_{ST} = \int_{x>0}\varphi_\rho^\dagger(x)[U_S(x) + \alpha\,\hat{p}\cdot E\times\sigma]\varphi_\lambda(x). \qquad \text{(A2)}$$

Taking the Hermitian conjugate of the S equation ($x > 0$), we obtain

$$\varphi_\rho^\dagger(x)U_S(x) = \left[\epsilon - \frac{\hat{p}^2}{2m}\right]\varphi_\rho^\dagger(x) + \alpha\,\hat{p}\varphi_\rho^\dagger(x)\cdot E\times\sigma \qquad \text{(A3)}$$

and $\epsilon = \epsilon_\lambda = \epsilon_\rho$ for elastic tunneling. Note that with partial integration, $\hat{p}\cdot E\times\sigma$ is Hermitian, however, to keep track of surface terms, we avoid now partial integration and keep the form $+\hat{p}\varphi_\rho^\dagger(x)$, using $\hat{p}^* = -\hat{p}$:

$$\begin{aligned}w_{ST} &= \int_{x>0}\varphi_\rho^\dagger(x)\epsilon\varphi_\lambda(x) - \int_{x>0}\left[\frac{p^2}{2m}\varphi_\rho^\dagger(x)\right]\varphi_\lambda(x)\\ &\quad + \alpha\int_{x>0}[\hat{p}\varphi_\rho^\dagger(x)]\cdot E\times\sigma]\varphi_\lambda(x)\\ &\quad + \alpha\int_{x>0}\varphi_\rho^\dagger(x)[\hat{p}\cdot E\times\sigma]\varphi_\lambda(x). \qquad \text{(A4)}\end{aligned}$$

Now $\epsilon\varphi_\lambda(x) = [\frac{p^2}{2m} + U_T(x)\theta(-x)]\varphi_\lambda(x)$ so that for $x > 0$,

$$\begin{aligned}w_{ST} &= \int_{x>0}\left\{\varphi_\rho^\dagger(x)\frac{p^2}{2m}\varphi_\lambda(x) - \left[\frac{p^2}{2m}\varphi_\rho^\dagger(x)\right]\varphi_\lambda(x)\right\}\\ &\quad + \alpha\int_{x>0}\hat{p}[\varphi_\rho^\dagger(x)\cdot E\times\sigma\varphi_\lambda(x)]. \qquad \text{(A5)}\end{aligned}$$

The first term gives Bardeen's formula

$$\begin{aligned}w_0 &= -\frac{\hbar^2}{2m}\int_{x>0}\nabla\{\varphi_\rho^\dagger(x)\nabla\varphi_\lambda(x) - [\nabla\varphi_\rho^\dagger(x)]\varphi_\lambda(x)\}\\ &= -\frac{\hbar^2}{2m}\int_S\{\varphi_\rho^\dagger(x)\nabla\varphi_\lambda(x) - [\nabla\varphi_\rho^\dagger(x)]\varphi_\lambda(x)\}\cdot\mathbf{dS}. \qquad \text{(A6)}\end{aligned}$$

The spin-orbit term reduces also to a surface term:

$$\begin{aligned}w_1 &= -i\alpha\cdot\int_S\varphi_\rho^\dagger(x)E\times\sigma\varphi_\lambda(x)\cdot\mathbf{dS}\\ &\approx w_0\cdot\frac{2m}{\hbar^2}\xi\alpha E\times\sigma\cdot\hat{n}, \qquad \text{(A7)}\end{aligned}$$

where $\hat{n}$ is a unit vector perpendicular to the surface and ξ is the scale generated by the gradient term in Eq. (A6). We note that w_1 does not need the assumption of equal masses as needed for w_0. For an "s-wave model" for the tip [34], there are scales $1/q$ of order of the tip size, $\sim$1 nm. These longer scales involve dS_x (parallel to the substrate), hence perpendicular to the field E, as needed for w_1. The large electric field under the STM tip can significantly enhance w_1. This shows that the tunneling element is in general a matrix in spin space.

APPENDIX B: KELDYSH FORMALISM

1. Green's functions and current

Within the Keldysh formalism, instead of the usual time-ordering operator used in equilibrium theory a contour-ordering operator, which orders time labels according to their order on the Keldysh contour, is introduced. For this problem, the single-particle propagators read

$$\begin{aligned}iG_{\sigma;\sigma'}(t,t') &= \langle T_{\mathcal{C}}[d_\sigma(t)d_{\sigma'}^\dagger(t')]\rangle,\\ iG_{\sigma;k\alpha,\sigma'}(t,t') &= \langle T_{\mathcal{C}}[d_\sigma(t)c_{k\alpha,\sigma'}^\dagger(t')]\rangle, \qquad \text{(B1)}\\ iG_{k\alpha,\sigma;k\beta,\sigma'}(t,t') &= \langle T_{\mathcal{C}}[c_{k\alpha,\sigma}(t)c_{k\beta,\sigma}^\dagger(t')]\rangle.\end{aligned}$$

The contour-ordered Green's function contains four different functions depending on where the times t and t' are over the Keldysh contour. It is easy to see that they are not all independent. We then consider the *lesser*, *greater*, and *retarded* Green's functions:

$$\begin{aligned}iG_{\sigma;\sigma'}^<(t,t') &= -\langle d_{\sigma'}^\dagger(t')d_\sigma(t)\rangle,\\ iG_{\sigma;\sigma'}^>(t,t') &= \langle d_\sigma(t)d_{\sigma'}^\dagger(t')\rangle, \qquad \text{(B2)}\\ iG_{\sigma;\sigma'}^R(t,t') &= \Theta(t-t')\langle[d_\sigma(t),d_{\sigma'}^\dagger(t')]_+\rangle,\end{aligned}$$

where $[,]_+$ denote the anticommutator of the fermionic operators and $\langle\cdots\rangle$ is the quantum statistical average. Analogous definitions apply to the other two single-particle propagators defined in (B1). These Green's functions can be evaluated after solving the Dyson equations.

In our model, the current operator in reservoir α (T or S) at time t has two components $\hat{J}_\alpha(t) = \hat{J}_{M\to\alpha}(t) + \hat{J}_{\overline{\alpha}\to\alpha}(t)$, being

$$\begin{aligned}\hat{J}_{M\to\alpha}(t) &= i\sum_{k\alpha,\sigma,\sigma'}\left(w_{\sigma,\sigma'}^\alpha\hat{c}_{k\alpha,\sigma}^\dagger(t)\hat{d}_{\sigma'}(t) - \text{H.c.}\right),\\ \hat{J}_{\overline{\alpha}\to\alpha}(t) &= i\,W\sum_{k\alpha,k\overline{\alpha},\sigma}(\hat{c}_{k\alpha,\sigma}^\dagger(t)e^{is_\alpha\sigma\phi_1}\hat{c}_{k\overline{\alpha},\sigma}(t) - \text{H.c.}),\end{aligned} \qquad \text{(B3)}$$

with $\overline{T} = S$ and $\overline{S} = T$ and $s_T = -s_S = 1$. The first line of (B3) corresponds to the current flowing through the molecule while the second one corresponds to the direct current between reservoirs.

The ensuing connected contour-ordered propagator reads in this case

$$iC_{\alpha\beta}(t,t') = \langle T_C[\hat{J}_\alpha(t)\hat{J}_\beta(t')]\rangle - \langle \hat{J}_\alpha(t)\rangle\langle \hat{J}_\beta(t')\rangle, \tag{B4}$$

while the *lesser*, *greater*, and *retarded* Green's functions are

$$\begin{aligned} iC^<_{\alpha\beta}(t,t') &= \langle \hat{J}_\beta(t')\hat{J}_\alpha(t)\rangle - \langle \hat{J}_\alpha(t)\rangle\langle \hat{J}_\beta(t')\rangle, \\ iC^>_{\alpha\beta}(t,t') &= \langle \hat{J}_\alpha(t)\hat{J}_\beta(t')\rangle - \langle \hat{J}_\alpha(t)\rangle\langle \hat{J}_\beta(t')\rangle, \\ iC^R_{\alpha\beta}(t,t') &= \Theta(t-t')\langle [\hat{J}_\alpha(t),\hat{J}_\beta(t')]_-\rangle, \end{aligned} \tag{B5}$$

where $[,]_-$ denote the commutator of the currents.

For the case of harmonic driving, it is convenient to use the Floquet-Fourier representation of the Green's functions [35]:

$$A_{j,j'}(t,t-\tau) = \sum_{k=-\infty}^{\infty}\int_{-\infty}^{\infty}\frac{d\omega}{2\pi}e^{-i(k\Omega_0 t+\omega\tau)}A_{j,j'}(k,\omega), \tag{B6}$$

where A stands for single-particle (B1) or current-current (B4) propagators.

2. Noise calculation

Although we are interested in the case of local current correlations, let us start by considering the more general case of correlation at different points. If we consider two reservoirs (α and β) and two times (an absolute time t and a relative time τ), we can define the nonsymmetrized correlation function of currents as

$$P_{\alpha\beta}(t,t-\tau) = \langle \Delta\hat{J}_\alpha(t)\Delta\hat{J}_\beta(t-\tau)\rangle, \tag{B7}$$

where $\Delta\hat{J}_\alpha(t) = \hat{J}_\alpha(t) - \langle\hat{J}_\alpha(t)\rangle$. This correlation function may be decomposed as

$$P_{\alpha\beta}(t,t-\tau) = \sum_{l(j)=M,\overline{\alpha}(\overline{\beta})} P^{l,j}_{\alpha\beta}(t,t-\tau), \tag{B8}$$

being

$$P^{l,j}_{\alpha\beta}(t,t-\tau) = \langle \Delta\hat{J}_{l\to\alpha}(t)\Delta\hat{J}_{j\to\beta}(t-\tau)\rangle, \tag{B9}$$

with $l(j) = M,\overline{\alpha}(\overline{\beta})$. With the definition of the contour-ordered current-current correlation function given in Eq. (B4), the correlation function of currents given in Eq. (B9) can be expressed as

$$P^{l,j}_{\alpha\beta}(t,t-\tau) = iC^{l,j;>}_{\alpha\beta}(t,t-\tau), \tag{B10}$$

where $iC^{l,j}_{\alpha\beta}(t,t-\tau)$ is defined as in (B4) but with the currents $\hat{J}_{l\to\alpha}(t)$ and $\hat{J}_{j\to\beta}(t-\tau)$.

Since experimentally the noise spectrum is averaged over the absolute time t, the relevant quantity here is

$$\mathcal{S}^{l,j}_{\alpha\beta}(\omega) = 2\int d\tau\left\langle P^{l,j}_{\alpha\beta}(t,t-\tau)\right\rangle_t e^{i\omega\tau}, \tag{B11}$$

where $\langle\ldots\rangle_t$ denotes the time average. From the definition of the Floquet-Fourier components given in Eq. (B6), it is easy to see that

$$\mathcal{S}^{l,j}_{\alpha\beta}(\omega) = iC^{l,j;>}_{\alpha\beta}(0,\omega). \tag{B12}$$

Hence the only relevant Floquet-Fourier component is the one with $k=0$. For the stationary situation, there is no t dependence and the result is just $iC^{l,j;>}_{\alpha\beta}(\omega)$.

Here, we present the final result for the different components of the noise spectrum in terms of the Floquet-Fourier representation of the Green's functions (B6). The calculation is similar to the one in Ref. [32]:

$$\begin{aligned}
\mathcal{S}^{M,M}_{\alpha\beta}(\omega) &= -\sum_k\int\frac{d\omega'}{2\pi}\mathrm{Tr}[\tilde{w}_\alpha\tilde{G}^{>;0,\beta}(k,\omega'+\omega)\tilde{w}_\beta\tilde{G}^{<;0,\alpha}(-k,\omega'_k) - \tilde{w}_\alpha G^>(k,\omega'+\omega)\tilde{w}^\dagger_\beta\tilde{G}^{<;\beta,\alpha}(-k,\omega'_k) \\
&\quad + \{>\leftrightarrow<;\omega\leftrightarrow-\omega\}^\dagger], \\
\mathcal{S}^{M,\overline{\beta}}_{\alpha\beta}(\omega) &= -\sum_k\int\frac{d\omega}{2\pi}\mathrm{Tr}[\tilde{w}_\alpha G^{>;0,\beta}(k,\omega'+\omega)\tilde{W}_\beta\tilde{G}^{<;\overline{\beta},\alpha}(-k,\omega'_k) - \tilde{w}_\alpha\tilde{G}^{>;0,\overline{\beta}}(k,\omega'+\omega)\tilde{W}^\dagger_\beta\tilde{G}^{<;\beta,\alpha}(-k,\omega'_k) \\
&\quad + \{>\leftrightarrow<;\omega\leftrightarrow-\omega\}^\dagger], \\
\mathcal{S}^{\overline{\alpha},M}_{\alpha\beta}(\omega) &= -\sum_k\int\frac{d\omega}{2\pi}\mathrm{Tr}[\tilde{W}_\alpha\tilde{G}^{>;\overline{\alpha},\beta}(k,\omega'+\omega)\tilde{w}_\beta\tilde{G}^{<;0,\alpha}(-k,\omega'_k) - \tilde{W}^\dagger_\alpha\tilde{G}^{>;\alpha,\beta}(k,\omega'+\omega)\tilde{w}_\beta\tilde{G}^{<;0,\overline{\alpha}}(-k,\omega'_k) \\
&\quad + \{>\leftrightarrow<;\omega\leftrightarrow-\omega\}^\dagger], \\
\mathcal{S}^{\overline{\alpha},\overline{\beta}}_{\alpha\beta}(\omega) &= -\sum_k\int\frac{d\omega}{2\pi}\mathrm{Tr}[\tilde{W}_\alpha\tilde{G}^{>;\overline{\alpha},\beta}(k,\omega'+\omega)\tilde{W}_\beta\tilde{G}^{<;\overline{\beta},\alpha}(-k,\omega'_k) - \tilde{W}_\alpha\tilde{G}^{>;\overline{\alpha},\overline{\beta}}(k,\omega'+\omega)\tilde{W}^\dagger_\beta\tilde{G}^{<;\beta,\alpha}(-k,\omega'_k) \\
&\quad + \{>\leftrightarrow<;\omega\leftrightarrow-\omega\}^\dagger],
\end{aligned} \tag{B13}$$

where Tr[...] is taken over the spin degrees of freedom and

$$\begin{aligned}
&(\tilde{w}_\alpha)_{\sigma,\sigma'} = w^\alpha_{\sigma,\sigma'}, \quad (\tilde{W}_\alpha)_{\sigma,\sigma'} = \delta_{\sigma,\sigma'}We^{is_\alpha\sigma\phi_1}, \quad (\tilde{G}(k,\omega))_{\sigma,\sigma'} = G_{\sigma;\sigma'}(k,\omega), \\
&(\tilde{G}^{0,\alpha}(k,\omega))_{\sigma,\sigma'} = \sum_{k\alpha}G_{\sigma;k\alpha,\sigma'}(k,\omega), \quad (\tilde{G}^{\alpha,\beta}(k,\omega))_{\sigma,\sigma'} = \sum_{k\alpha,k\beta}G_{k\alpha,\sigma;k\beta,\sigma'}(k,\omega).
\end{aligned} \tag{B14}$$

The two components of the noise spectrum $\mathcal{S}_M$ and $\mathcal{S}_W$ in (11) correspond to $\mathcal{S}^{M,M}_{T,T} + \mathcal{S}^{M,S}_{T,T} + \mathcal{S}^{S,M}_{T,T}$ and $\mathcal{S}^{S,S}_{T,T}$ in (B13), respectively.

[1] A. V. Balatsky, M. Nishijima, and Y. Manassen, Adv. Phys. **61**, 117 (2012).

[2] D. Rugar, R. Budakian, H. J. Mamin, and B. W. Chui, Nature (London) **430**, 329 (2004).

[3] Y. Manassen, R. J. Hamers, J. E. Demuth, and A. J. Castellano Jr., Phys. Rev. Lett. **62**, 2531 (1989).

[4] Y. Manassen, E. Ter-Ovanesyan, D. Shachal, and S. Richter, Phys. Rev. B **48**, 4887 (1993).

[5] Y. Manassen, I. Mukhopadhyay, and N. R. Rao, Phys. Rev. B **61**, 16223 (2000).

[6] C. Durkan and M. E. Welland, Appl. Phys. Lett. **80**, 458 (2002).

[7] P. Messina, M. Mannini, A. Caneschi, D. Gatteschi, L. Sorace, P. Sigalotti, C. Sandrin, P. Pittana, and Y. Manassen, J. Appl. Phys. **101**, 053916 (2007).

[8] M. Mannini, P. Messina, L. Sorace, L. Gorini, M. Fabrizioli, A. Caneschi, Y. Manassen, P. Sigalotti, P. Pittana, and D. Gatteschi, Inorganica Chimica Acta **360**, 3837 (2007).

[9] V. Mugnaini, M. Fabrizioli, I. Ratera, M. Mannini, A. Caneschi, D. Gatteschi, Y. Manassen, and J. Veciana, Sol. St. Sci. **11**, 956 (2009).

[10] T. Komeda and Y. Manassen, Appl. Phys. Lett. **92**, 212506 (2008).

[11] Y. Sainoo, H. Isshiki, S. M. F. Shahed, T. Takaoka, and T. Komeda, Appl. Phys. Lett. **95**, 082504 (2009).

[12] Y. Manassen, M. Averbukh, and M. Morgenstern, Surf. Sci. **623**, 47 (2014); Y. Manassen (private communication).

[13] D. Mozyrsky, L. Fedichkin, S. A. Gurvitz, and G. P. Berman, Phys. Rev. B **66**, 161313 (2002).

[14] L. N. Bulaevskii, M. Hruska, and G. Ortiz, Phys. Rev. B **68**, 125415 (2003).

[15] S. A. Gurvitz, D. Mozyrsky, and G. P. Berman, Phys. Rev. B **72**, 205341 (2005).

[16] O. Entin-Wohlman, Y. Imry, S. A. Gurvitz, and A. Aharony, Phys. Rev. B **75**, 193308 (2007).

[17] A. V. Balatsky, Y. Manassen, and R. Salem, Phil. Mag. B **82**, 1291 (2002); Phys. Rev. B **66**, 195416 (2002).

[18] Y. Manassen and A. V. Balatsky, Isr. J. Chem. **44**, 401 (2004).

[19] L. S. Levitov and E. I. Rashba, Phys. Rev. B **67**, 115324 (2003).

[20] R. López, D. Sánchez, and L. Serra, Phys. Rev. B **76**, 035307 (2007).

[21] J. Bork, Y. Zhang, L. Diekhöner, L. Borda, P. Simon, J. Kroha, P. Wahl, and K. Kern, Nat. Phys. **7**, 901 (2011).

[22] I. J. Hamad, L. Costa Ribeiro, G. B. Martins, E. V. Anda, Phys. Rev. B **87**, 115102 (2013).

[23] A. Muller, E. B. Flagg, P. Bianucci, X. Y. Wang, D. G. Deppe, W. Ma, J. Zhang, G. J. Salamo, M. Xiao, and C. K. Shih, Phys. Rev. Lett. **99**, 187402 (2007).

[24] S. M. Ulrich, S. Ates, S. Reitzenstein, A. Löffler, A. Forchel, and P. Michler, Phys. Rev. Lett. **106**, 247402 (2011).

[25] L. D. Landau and E. M. Lifshitz, *Quantum Mechanics*, 3rd ed., A Course of Theoretical Physics Vol. 3 (Pergamon Press, New York, 1977).

[26] Ya. M. Blanter and M. Büttiker, Phys. Rep. **336**, 1 (2000).

[27] H. Birk, M. J. M. de Jong, and C. Schönenberger, Phys. Rev. Lett. **75**, 1610 (1995).

[28] J. Ferrer, A. Martín-Rodero, and F. Flores, Phys. Rev. B **38**, 10113 (1988).

[29] B. Rizzo, L. Arrachea, and J. P. Paz, Phys. Rev. B **85**, 045442 (2012).

[30] E. A. Rothstein, O. Entin-Wohlman, and A. Aharony, Phys. Rev. B **79**, 075307 (2009).

[31] A. Golub and B. Horovitz, Phys. Rev. B **88**, 115423 (2013).

[32] A. Caso. L. Arrachea and G. Lozano, Eur. Phys. Jour. B **85**, 266 (2012).

[33] J. Bardeen, Phys. Rev. Lett. **6**, 57 (1961).

[34] C. J. Chen, Phys. Rev. B **42**, 8841 (1990).

[35] L. Arrachea and M. Moskalets, Phys. Rev. B **74**, 245322 (2006); L. Arrachea, *ibid.* **75**, 035319 (2007).